Proceedings of the ASME 2010 3rd Joint US-European Fluids Engineering Summer Meeting and 8th International Conference on Nanochannels, Microchannels, and Minichannels
FEDSM-ICNMM2010
August 1-5, 2010, Montreal, Canada

FEDSM-ICNMM2010-30740

EXPERIMENTAL STUDY OF STRUCTURE AND DYNAMICS OF TURBULENT STRATIFIED JET

Duo Xu and Jun Chen

School of Mechanical Engineering
Purdue University
West Lafayette, Indiana, 47907, U.S.A.

ABSTRACT

Stratified flows are frequently observed in environmental and oceanic applications, which often involve interaction of momentum and scalar flux. In this study, Particle Image Velocimetry and Planar Laser Induced Fluorescence are applied to simultaneously measure the velocity and density fields of a turbulent jet discharged horizontally into an environment with density difference, for studying the mixing and entrainment process in stratified flows. The data are analyzed to gain understanding of the physical mechanism of vertical mixing (mixing along gravity direction) and horizontal mixing (mixing along horizontal direction) introduced by the turbulent jet flows. The dataset also provides a test platform for mixing models used in stratified flow simulations.

NOMENCLATURE

U_0: initial centerline velocity at nozzle exit, $U_0 = \langle U(0,0,0)\rangle$

U_c: the centerline velocity, $U_c(x) = \langle U(x,0,0)\rangle$

ρ_e: density of light fluid

ρ_s: density of dense fluid

g_s: grayscale value of image

c: concentration of fluorescence dye

c_0: initial fluorescence dye concentration

$\Delta\rho_0 = \rho_s - \rho_e$: initial density difference between light and dense fluids

g: gravitional acceleration

$g' = g \cdot \Delta\rho/\rho$: reduced gravity

D: diameter of nozzle exit

$R_i = g'D/U_0^2$: (bulk) Richardson number

μ: viscosity of fluid

$R_e = \rho_s U_0 D/\mu$: (bulk) Reynolds Number

$\theta = \Delta\rho/\Delta\rho_0$: non-dimensional density difference

$\theta_c(x) = \langle\theta(x,0,0)\rangle$: non-dimensional centerline density difference

$y_{1/2}$: velocity half-width in horizontal plane

$z_{\pm 1/2}$: velocity half-width in vertical plane

$y^{\theta}_{1/2}$: density half-width in horizontal plane

$z^{\theta}_{\pm 1/2}$: density half-width in vertical plane

Ω_y: vorticity along Y direction

INTRODUCTION

Stratified flows exist extensively in environmental and geophysical applications. For example, ocean flows are described as a thin stratified fluid using hydrostatic and Boussinesq approximations in global-scale ocean simulations [1], and the discharge of sewage water into ocean forms a stratified current that has density difference than the ambient ocean water. Particularly, developing effective mixing models for numerical simulations presents a major challenge and it requires a better understanding of the underlying physics of density (scalar) mixing and entrainment process in stratified turbulent flows [2–5]. To investigate this problem through laboratory experiments, needed are simultaneous measurements of velocity and density fields, which make analysis of mixing and entrainment feasible.

In the past, various experimental efforts of measuring scalar (concentration or density) field and velocity field are reported. For example, Webster and Liu [6] apply digital particle tracking velocimetry to investigate the behavior of a horizontal turbulent round jet injected into a linearly stratified environment. A planar laser-induced fluorescence (PLIF) technique is used by Crimaldi and Koseff [7] to measure the the scalar spatial structure of turbulent flows at high resolution. Papanicolao et al. [8] use PLIF and laser Doppler anemometry to study the velocity components, as well as the concentration distribution, of a turbulent buoyant jet. Dahm and Dimotakist [9] investigate the entrainment and mixing in the self-similar far field of a turbulent jet in water by applying PLIF to measure the time-varying fluid concentration field. Particle Image Velocimetry (PIV) is applied by Kwon and Seo to study Reynolds number effects on the behavior of a non-buoyant round water jet [10]. PIV and PLIF are combined to measure the concentration field and velocity field simultaneously, by Wang and Law [11, 12] to study the buoyant jet discharges, by Zarruk and Cowen [13] to investigate a neutrally buoyant turbulent round jet at two Reynolds numbers, and by Feng et al. [14] to study a confined liquid-phase rectangular jet.

In this paper, we describe a laboratory experiment for studying the structure and dynamics of a turbulent stratified jet, which serves as a model problem for investigating mixing and entrainment process of stratified flow. Moreover, we conduct measurement in vertical direction (parallel to the buoyancy direction) and in horizontal direction (perpendicular to the buoyancy direction), to gain understanding of isotropy of mixing process. Details about the facility are presented in section 2. Instrumentation techniques are introduced in section 3. In section 4, the results are discussed. The final section gives a summary and outlook.

EXPERIMENTAL FACILITY

The core part of the facility is consisted of a main tank and a jet nozzle as shown in figure 1. The main tank with dimensions of $122 \times 30 \times 30$ cm^3, is made of 1.27 cm thick acrylic plates, and it is filled with light fluid (ethanol solution with density ρ_e). The jet nozzle is made of acrylic pipe with the inner diameter 1.27 cm. It is connected to an upstream diffuser which is manufactured using 3D jet printing technique. The diffuser is used to eliminate the inlet flow fluctuation to generate the turbulent jet flow with nearly uniform and stable velocity profile. A constant head system (not shown in figure 1), including a head-control tank, a supply tank and two centrifugal pumps, is filled with dense fluid (salt solution with density ρ_s). A centrifugal pump (1750 RPM, 1/55 Hp), connected to the constant head system, generates a jet of dense fluid into the light fluid in the main tank, at a flow rate 0.24 L/s. Also as shown in figure 1, a piece of polycarbonate honeycomb (thickness 7.5 cm, hole diameter 3 mm) is placed at the far end of the tank to eliminate the influence of secondary flow reflected by the end wall. Another piece of honeycomb (thickness 5.0 cm, hole diameter 3 mm) is placed in the main tank to eliminate the surface wave.

The origin of the coordinate system is set at the center of the jet exit plane, shown in figure 1, while the X axis is set horizontally along the flow direction and the Y axis is set to be perpendicular to the X axis in the horizontal plane, and Z axis points upwardly normal to the X-Y plane, i.e., Z axis is anti-parallel to gravitional direction.

INSTRUMENTATION

The difference of refractive indices of dense liquid and light liquid, caused by the density difference, leads to unfocused image in optical measurements, which deteriorates the acuracy of optical measurement. In order to apply optical flow diagnostics techniques in stratified flows, the refractive indices of the dense fluid and light fluid must be matched [15–18]. In our experiments we use salt solution as the dense fluid and ethanol solution as the light fluid, and

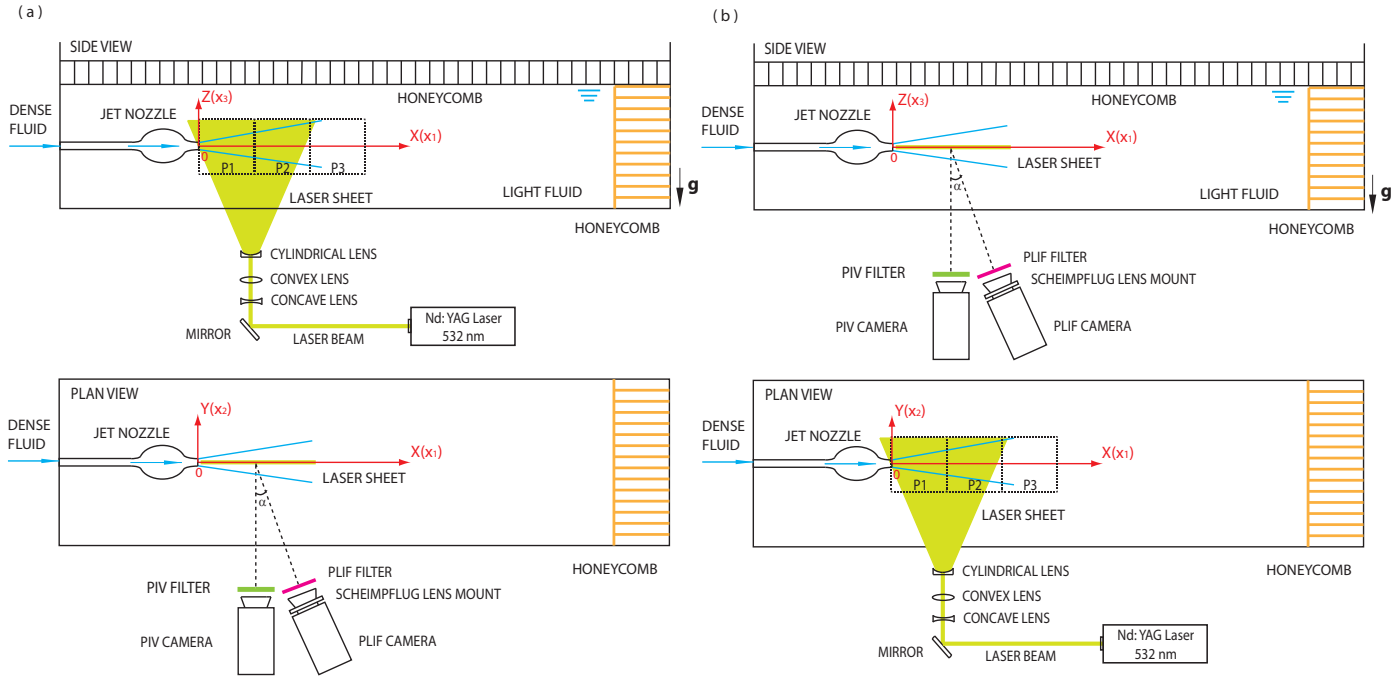

Figure 1. Schematic illustration of the Stratified Turbulent Jet Flow Facility for (a) Vertical Mixing and (b) Horizontal Mixing.

match their refractive indices. The densities and refractive indices of the fluids are measured by a densitometer (Mettler Toledo Densito 30PX) and a refractometer (Mettler Toledo Refracto 30PX).

Particle Image Velocimetry and Planar Laser Induced Fluorescence are applied to measure the velocity and density simultaneously. A dual-head Nd: YAG laser (Big Sky Laser Twins BSL, wavelength 532 nm, peak energy 130 mJ/pulse) is used to generate a 1 mm thick laser sheet through a group of lenses in the test section.

The dense and light fluids are seeded with hollow glass beads (median diameter 11 μm, specific gravity 1.1). A PIV camera (14-bit Imager ProX 4M CCD camera) of 2048 $\times$ 2048 pixels resolution is used to record the PIV images, operated under double exposure mode at a sampling rate of 5 Hz. The time delay between a pair of laser pulses is set to from 400 μs to 600 μs, depending on the averaged flow velocity in the sample area. Velocity vectors are retrieved by processing image pairs by using PIV analysis software (Davis). A two-step processing is applied: 64 $\times$ 64 pixels interrogation window and 50% overlap for the first step, and 32 $\times$ 32 pixels interrogation window and 50% overlap for the second step. Thus, a total of 128 $\times$ 128 vectors are resolved from each PIV image pair. The sample area of PIV measurement is 11.0$\times$11.0 cm^2, and the spatial resolution is 0.0875 cm.

To apply PLIF measurement, a fluorescent dye, Rhodamine 6G, is mixed uniformly in the dense fluid. The dye serves as a surrogate of the concentration of dense fluid mixed into light fluid, i.e., the local dye concentration is of a linear relationship with the local density of the mixture. The Rhodamine 6G absorbs the excitation light of center around 530 nm and emits fluorescence with a peak at 550 nm [19]. In the present experiment, the same pulse laser is used to excite the fluorescence and to illuminate PIV particles, as shown in figure 1. The PLIF images are recorded by a PLIF camera (14-bit Imager ProX 4M CCD camera) with 2048 $\times$ 2048 pixels resolution. As shown in figure 1, this camera points to the test section at a tilt angle α (about 15°). A scheimpflug lens mount is used on this camera to keep the PLIF image focused.

The grayscale value in the PLIF image, g_s, is a function

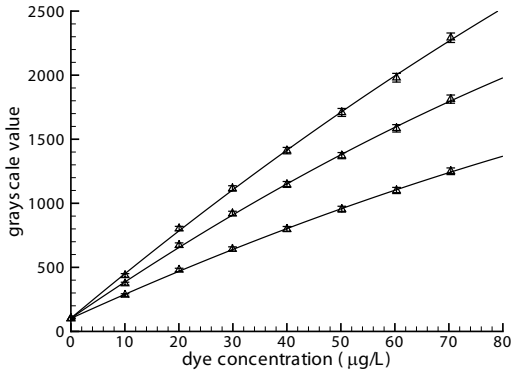

Figure 2. Three typical PLIF calibration curves. Each curve is corresponding to a pixel location in the PLIF image. Symbols show the averaged value from 50 calibration images and the error bars show the rms values.

of the dye concentration value, c:

$$g_s(x,y,z,t) = f(c(x,y,z,t)), \tag{1}$$

if the excitation intensity is assumed constant. This relationship between the g_s and c is determined by calibration procedure, in which PLIF images of the sample area, with controlled dye concentration, are recorded. In the calibration for this study, 8 dye concentration levels, from 0 μg/L to 70 μg/L, are generated. A total of 50 images are recorded at each level. Then the data is curve fitted to establish a second order polynomial to relate g_s and c at every pixel location in the PLIF image. Thus, for a recorded g_s, a corresponding dye concentration c can be determined from the calibration curve. Furthermore, the density difference $\Delta\rho$ of the mixture is given by:

$$\Delta\rho(x,y,z,t) \equiv \rho(x,y,z,t) - \rho_e = \frac{c(x,y,z,t)}{c_0}\Delta\rho_0, \tag{2}$$

where c_0 is the initial fluorescence dye concentration in the dense liquid (e.g., c_0=60 μg/L) and $\Delta\rho_0 = \rho_s - \rho_e$.

To measure the velocity fields and density fields simultaneously, PIV and PLIF signals are separated. A PIV filter (bandpass, center wavelength 530$\pm$10 nm) is applied to pass the scatter light from PIV particles and block the fluorescence signal. Another PLIF filter (highpass with cutoff 550 nm) is used to block the PIV signal and pass the fluorescence signal only. The sample area of PLIF measurement encloses the sample area of PIV measurement, so that the PLIF data can be subsampled to obtain the concentration field over the same grid as for PIV measurement, i.e., for every node among the 128×128 PIV grids, there is a velocity vector measured from PIV and a density value from PLIF.

We conduct two series of experiments on stratified turbulent jet, using the above-mentioned PIV-PLIF measurement: one for vertical mixing along the vertical central plane (Y=0, shown in figure 1-a), and another for horizontal mixing along the horizontal central plane (Z=0, shown in figure 1-b). The positions and orientations of PIV and PLIF cameras and laser sheet orientation are different, as shown in the figure 1. Measurement at three consecutive downstream locations (along the X direction, labeled as P1-P3 in figure 1), are conducted for both the vertical mixing and horizontal mixing cases. At each location, a total of 600 repeated PIV-PLIF measurements are recorded, from 4 runs, to form an ensemble set for statistical analysis. During each run, the effective data acquisition time is 30 seconds and the height change of the free surface is ignorable within this time. After each run, the main tank is drained and rinsed to remove the residual fluorescence dye. Then the liquids are prepared again for next experiment run.

RESULTS

The stratified data discussed in this paper are obtained from the following experimental conditions: characteristic inject velocity $U_0 = 1.9$ m/s; Reynolds number $R_e = \rho_s U_0 D/\mu = 20000$; initial relative density difference $\Delta\rho_0/\rho_e = 0.5\%$; and initial bulk Richardson number $R_i = g'D/U_0^2 = 1.7 \times 10^{-4}$. This dataset is referred to as "stratified case". We also perform PIV measurement for another case where no initial density difference is created. In this controlled case (referred to as "unstratified case"), the inject velocity and the Reynolds number are the same as in the stratified case while the density difference is zero.

A typical snapshot of velocity and density fields is shown in figure 3. The development of the jet structure and dilution of dense fluid can be clearly identified. As the jet flow moves downstream, complicated mixing and entrainment structures appear around the outter edge of the jet. The ensemble averaged mean velocity $\langle U_i \rangle$ and density $\langle \rho \rangle$ are calculated from the 600 snapshots at each location.

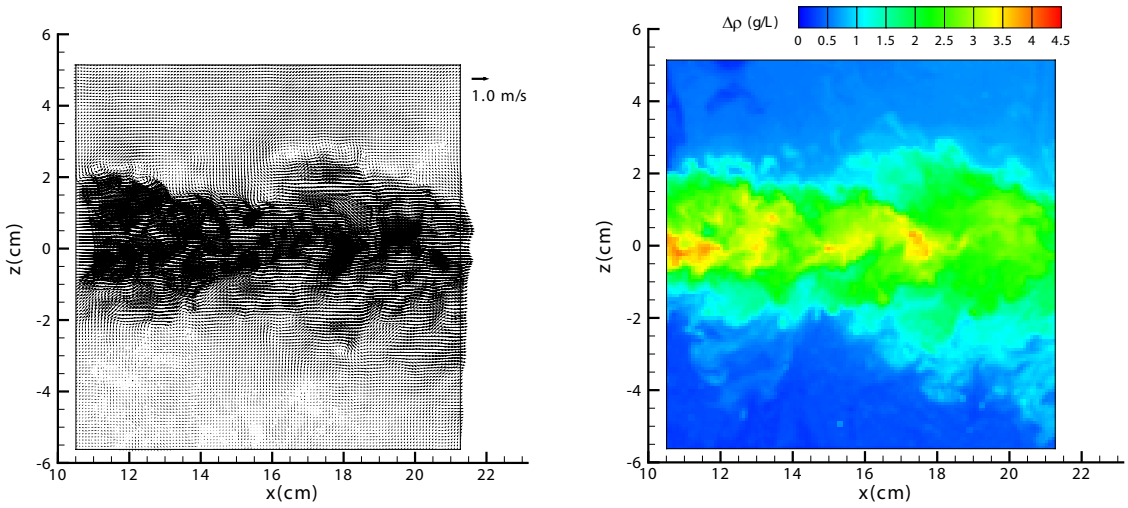

Figure 3. An snapshot of velocity (left) and density (right) fields of vertical measurement at P2.

Then the data from locations P1-P3 are jointed together to show the mean velocity and voriticity distributions from $X/D = 0$ to 24.

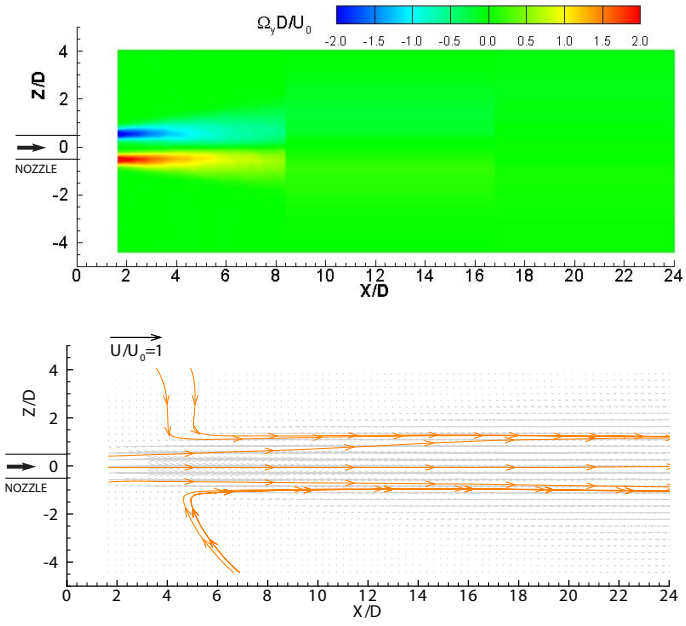

Figure 4. Distribution of the non-dimensional vorticity ($\Omega_y D/U_0$, top) and vectors and streamlines showing the mean flow pattern (bottom). The data is from vertical measurement of stratified case. For clarity only 1/16 of vectors are displayed.

In the present experiment, the streamwise (axial) velocity component $U(x,y,z)$ is much larger than the other two velocity components. The distribution of the mean vorticity in vertical stratified mixing case, as shown in figure 4, illustrates that strong vortices exist near the nozzle exit, which is caused by the mixing and entrainment near nozzle tip. Also displayed in figure 4 are the mean velocity vectors and streamlines showing the mean flow pattern.

To understand the development of the stratified jet, the vertical profiles of axial velocity component, at three typical downstream locations ($X/D = 8$, 16 and 24), are plotted in figure 5. The counterpart profiles of unstratified case are also plotted for comparision. The Z-location of the peak of the velocity profile occurs at $Z\sim0$, i.e., the centerline of the jet structures for both cases is nearly horizontal. For each location, the velocity profiles of stratified and unstratified cases do not overlap, although the initial density difference is only 0.5% and the Ricardson number is small ($R_i = 1.7 \times 10^{-4}$). The centerline mean velocity of stratified case is always larger than that of the unstratified case, and the difference ranges from 3.6% to 16.7%, for X/D=8 to 24. If we analyze the upper portion ($Z \geq 0$) and lower portion ($Z \leq 0$) of the velocity profiles seperately in the vertical mixing, we observe differences around the outter edge of the jet. For example, for X/D=16, when Z/D >1.0, $\langle U \rangle$ of the stratified case (diamond symbols in figure 5) is smaller than that of the unstratified case (diamond dash line in figure 5), while the trend is reversed when Z/D<-

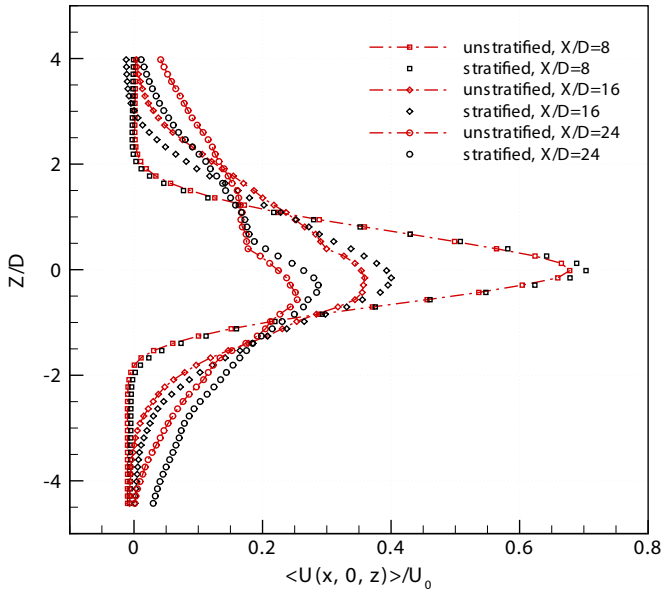

Figure 5. Vertical profiles of streamwise velocity component ($\langle U \rangle / U_0$) of stratified and unstratified cases at three different downstream locations.

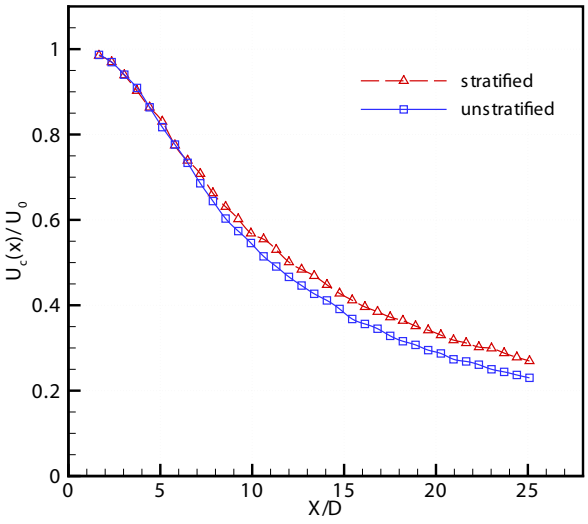

Figure 6. Development of the mean centerline velocity along X direction to compare the velocity decreasing difference between stratified and unstratified mixing.

1.6 along the same profiles. When $X/D = 24$, the difference described above is more evident. This observed difference is due to the following facts. In the upper portion, light liquid (ambient fluid, ρ_e) is on top of dense liquid (jet mixture, $\rho_e < \rho < \rho_s$) and this forms a stable stratification, which restrains the turbulent mixing. This less active mixing causes smaller mean axial velocity around the outer edge of the jet compared to the unstratified case. In the lower portion, on the contrary, the dense liquid is on top of light liquid and this forms an unstable stratification, which enhances the turbulent mixing. As a result, the mean axial velocity of stratified case is larger than that of the unstratified case.

To investigate the difference between stratified and unstratified cases, the centerline velocities, $U_c(x) = \langle U(x,0,0) \rangle$, are plotted as a function of x in figure 6. The centerline velocity of stratified case decreases at a slower rate than the unstratified case, which means the core part of the stratified case can loses les kinetic energy due to less dissipation compared to the unstratified case. In another word, the stratified case can maintain its momentum to travel a longer downstream distance.

The distribution of the ensemble averaged mean non-dimensional density difference $\theta = \Delta\rho/\Delta\rho_0$, of stratified vertical and horizontal mixing along the X direction is shown in figure 7 with the label of the non-dimensional density contour. We can observe the density change due to mixing and dilluting process as the jet structure developed. For the vertical mixing, the centerline density profiles departure from horizontal line (Z=0) as the jet travels to downstream. For the horizontal mixing, the profiles are nearly symmetric about X axis. This can be explained by the difference of buoyancy term in vertical and horizontal cases.

We apply the similarity analysis to the obtained dataset. The horizontal velocity half-width and vertical velocity half-width of the jet, $y_{1/2}$ and $z_{\pm 1/2}$, are defined such that $\langle U(x,y_{1/2},0) \rangle = \langle U(x,0,z_{+1/2}) \rangle = \langle U(x,0,-z_{-1/2}) \rangle = 1/2U_c(x)$ [20]. For the horizontal measurement, for both stratified and unstratified cases, as shown in figure 8, the profiles of $\langle U \rangle / U_c(x)$, plotted against $y/y_{1/2}$, collapse on a single curve. This suggests that a same similarity solution is nearly valid for both stratified and unstratified cases at the density difference being studied in the horizontal direction.

From the vertical measurement, there is a difference of the similarity profiles, as shown in figure 9. At a upper stream location (X/D=8), the curves of stratified and unstratified profiles nearly overlap each other. At this loca-

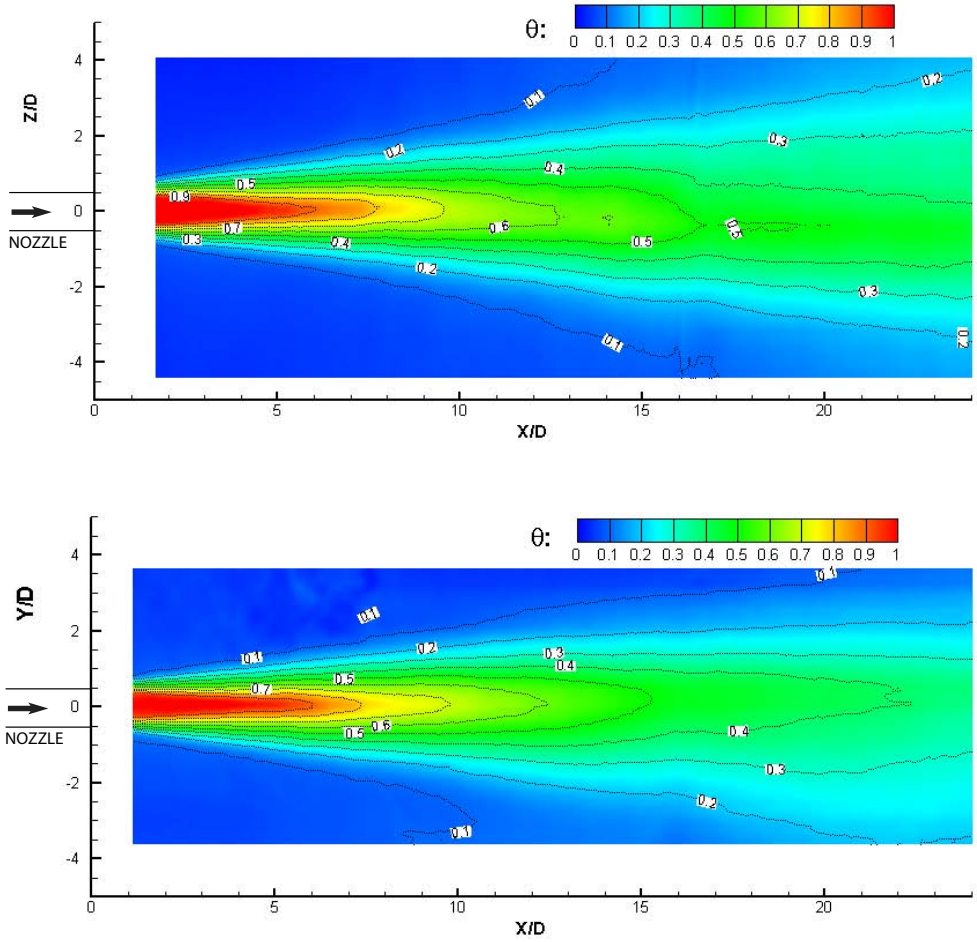

Figure 7. Schematic illustration of the distribution of the non-dimensional density difference θ of the stratified turbulent jet, the top figure is vertical mixing and the bottom figure is horizontal mixing.

tion the local R_i number is much smaller than unity, which means the turbulent mixing is dominant and influence of buoyancy is less important. However, at a downstream location (X/D=24), further away from nozzle exit, the profiles of $\langle U\rangle/U_c(x)$ in the stratified and unstratified cases are different. As also shown in figure 9, we analyze the profiles of upper portion and lower portion seperately. In the upper portion, at the same z, the value of $\langle U\rangle/U_c(x)$ of stratified case is smaller than that of the unstratified case for $z/z_{+1/2} > 1.2$, while in the lower portion, the value of $\langle U\rangle/U_c(x)$ of stratified case is larger than that of the unstratified case for $z/z_{-1/2} < -1.2$. The difference is caused by the stable and unstable stratification in the upper and lower portions, as discussed before.

We define a centerline density difference as $\theta_c(x) = \langle\theta(x,0,0)\rangle$, and the horizontal density half-width and vertical density half-width, $y^{\theta}_{1/2}$ and $z^{\theta}_{\pm 1/2}$, are defined in the the same way as for velocity half-width, i.e., $\langle\theta(x,y^{\theta}_{1/2},0)\rangle = \langle\theta(x,0,z^{\theta}_{+1/2})\rangle = \langle\theta(x,0,-z^{\theta}_{-1/2})\rangle = 1/2\theta_c(x)$. Figure 10 shows the ensemble averaged mean density of both vertical and horizontal stratified mixing against the radial distance at locations $X/D = 8$ and 16. At $X/D = 8$, the profiles of $\langle\theta\rangle/\theta_c(x)$ for horizontal mixing (square symbols) and vertical mixing (left triangle symbols) nearly collapse. At $X/D = 16$, further away from the nozzle exit, when $y/y_{1/2} > 1.2$ and $z/z_{1/2} > 1.2$, the profiles of $\langle\theta\rangle/\theta_c(x)$ for horizontal mixing, does not fit with the profiles for vertical mixing, and relative difference of $\langle\theta\rangle$ is about 25 %. Figure

11 shows that the profiles of $\langle\theta\rangle/\theta_c(x)$ for vertical mixing at three downstream locations does not collapse. This suggests that $\langle\theta\rangle/\theta_c(x)$ can not lead to a similarity solution of density distribution in stratified jet, at least in the outer edge of the jet where $z/z_{1/2} > 1.0$.

To understand the stratified jet expansion structure In figure 12, the development of velocity half-width ($y_{1/2}$ and $z_{\pm 1/2}$) and density half-width ($y^{\theta}_{1/2}$ and $z^{\theta}_{\pm 1/2}$) are plotted together as functions of x. The velocity half-width curves including stratified and unstratified, horizontal and vertical as well, are almost coincident. However, the density half-width curves of horizontal and vertical cases do not overlap each other and also larger than the values of velocity curves.

SUMMARY

A turbulent jet facility is developed to investigate the dynamics of unstratified and stratified mixing and entrainment process, at Reynolds number $R_e = 20000$ and Richardson number $R_i = 1.7 \times 10^{-4}$. A combined PIV-PLIF technique measures the 2D velocity and density fields simultaneously at high spatial resolution. Particularly studied are vertical mixing (within X-Z plane) and horizontal mixing (within X-Y plane), as well as the downstream development of jet structures. The ensemble averaged velocity and density are applied for similarity analysis. According to analysis and observation, there is a significant difference in the dynamics of the mixing and entrainment between the unstratified and stratified round jet even though the density difference of stratified case is only 0.5%. The velocity profiles of stratified and unstratified cases are almost the same along the horizontal direction, but stratified vertical mixing must be analyzed by upper portion

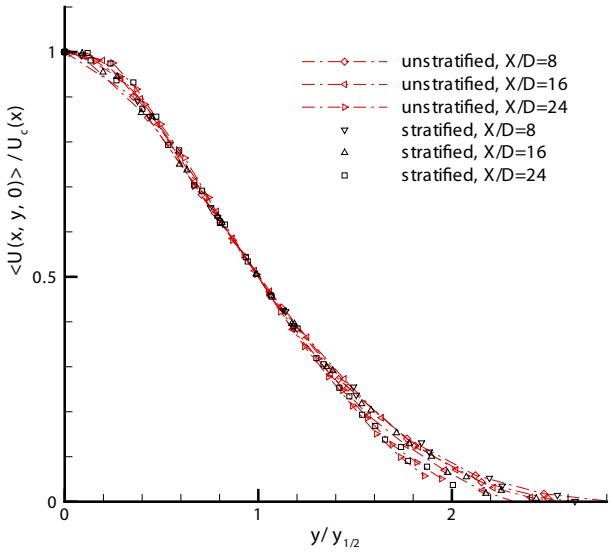

Figure 8. The ensemble averaged velocity against radial distance for the horizontal mixing of both stratified and unstratified jets.

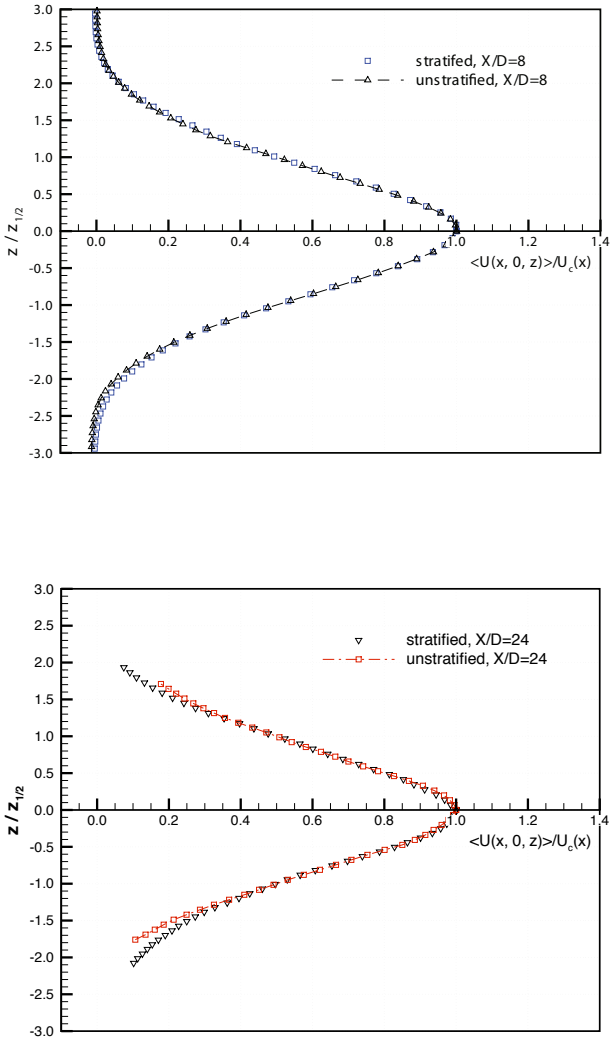

Figure 9. The ensemble average velocity against radial distance for the vertical mixing of both stratified and unstratified jets: (top) X/D=8 and (bottom) X/D=24.

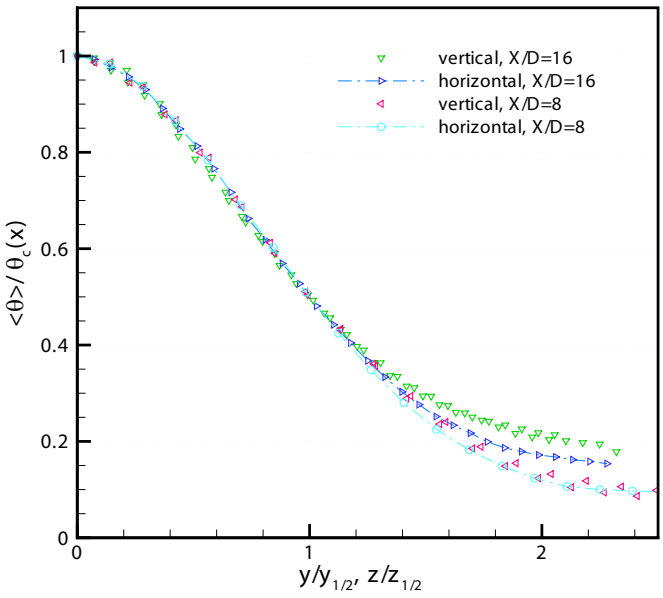

Figure 10. The ensemble averaged non-dimensional density against the radial distance at locations X/D=8 and 16 for both the vertical mixing and horizontal mixing cases.

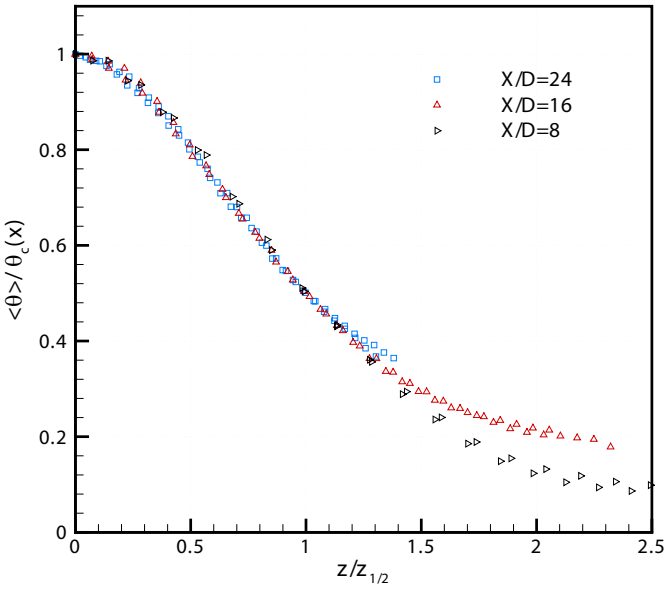

Figure 11. The ensemble averaged non-dimensional density against the radial distance of stratified vertical mixing at locations X/D=8, 16 and 24.

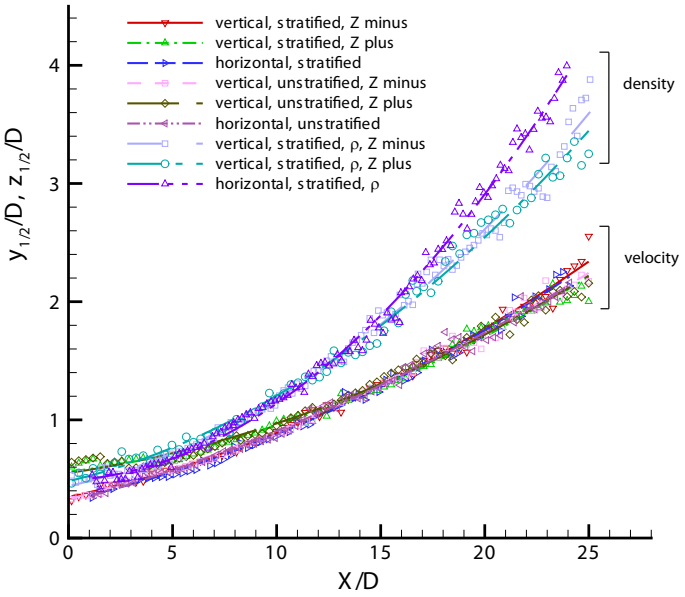

Figure 12. Schematic illustration of the half width radial distance along X direction.

(stable stratification) and lower portion (unstable stratification) seperately. A similarity solution can not be obtained to profiles of $\langle\theta\rangle/\theta_c(x)$, especially for outer edge of the jet. On-going efforts include change of Richardson Number and Reynolds Number by adjusting the experimental conditions, to better understand physics and modeling of stratified mixing.

REFERENCES

[1] Smith, R., and Gent, P., May 2002. Reference manual for the Parrallel Ocean Program (POP). Tech. Rep. LAUR-02-2484 (Los Alamos National Laboratory).

[2] Large, W. G., McWilliams, J. C., and Doney, S. C., 1994. "Oceanic vertical mixing: A reivew and a model with nonlocal boundary layer parameterization". *Review of Geophysics,* **32**, pp. 363–403.

[3] Ivey, G. N., Winters, K. B., and Koseff, J. R., 2008. "Density stratification, turbulence, but how much mixing?". *Ann. Rev. Fluid Mech.,* **40**, pp. 169–184.

[4] Stretch, D. D., Rottman, J. W., Venayagamoorthy, S. K., Nomura, K. K., and Rehmann, C. R., 2010. "Mixing efficiency in decaying stably stratified turbulence". *Dynamics of Atmospheres and Oceans,* **49**,

pp. 25–36.
[5] Muller, P., and Garrett, C., 2002. "From stirring to mixing in a stratified ocean". *Oceanography,* **15**, pp. 12–19.
[6] Webster, D. R., and Liu, Y., 2001. "Velocity measurements of turbulence collapse in a linearly stratified jet". *Exp. in Fluids,* **31**, pp. 394–400.
[7] Crimaldi, J. P., and Koseff, J. R., 2001. "High-resolution measurements of the spatial and temporal scalar structure of a turbulent plume". *Exp. in Fluids,* **31**, pp. 90–102.
[8] Papanicolaou, P., and List, E. J., 1998. "Investigations of round vertical turbulent buoyant jets". *J. Fluid Mech.,* **195**, pp. 341–391.
[9] Dahm, W. J. A., and Dimotakis, P. E., 1987. "Measurements of entrainment and mixing in turbulent jets". *AIAA Journal,* **25**, pp. 1216–1223.
[10] Kwon, S. J., and Seo, I. W., 2005. "Reynolds number effects on the behavior of a non-buoyant round jet". *Exp. in Fluids,* **38**, pp. 801–812.
[11] Wang, H., 2000. "Investigations of buoyant jet discharges using combined dpiv and plif". PhD thesis, Nanyang Technological University, Singapore.
[12] Wang, H., and Law, A. W.-K., 2002. "Second-order integral model for a round turbulent buoyant jet". *J. Fluid Mech.,* **459**, pp. 397–428.
[13] Zarruk, G. A., and Cowen, E. A., 2008. "Simultaneous velocity and passive scalar concentration measurements in low reynolds number neutrally buoyant turbulent round jets". *Exp. in Fluids,* **44**, pp. 865–872.
[14] Feng, H., Olsen, M. G., Hill, J. C., and Fox, R. O., 2007. "Simultaneous velocity and cocentration field measurements of passive-scalar mixing in a confined rectangular jet". *Exp. in Fluids,* **42**, pp. 847–862.
[15] Daviero, G. J., Roberts, P. J. W., and Maile, K., 2001. "Refractive index matching in large-scale stratified experiments". *Exp. in Fluids,* **31**, pp. 119–126.
[16] Alahyari, A., and Longmire, E. K., 1994. "Particle image velocimetry in a variable density flow: application to a dynamically evolving microburst". *Exp. in Fluids,* **17**, pp. 434–440.
[17] Hannoun, I., Fernando, H., and List, E., 1988. "Turbulent structure near a sharp density interface". *J. Fluid Mech.,* **189**, pp. 189–209.
[18] McDougall, T., 1979. "On the elimination of refractive-index variations in turbulent density-stratified liquid flows". *J. Fluid Mech.,* **93**, pp. 83–96.
[19] Du, H., Fuh, R. A., Li, J., Corkan, A., and Lindsey, J. S., 1998. "PhotochemCAD: A computer-aided design and research tool in photochemistry". *Photochemistry and Photobiology,* **68**, pp. 141–142.
[20] Pope, S. B., 2001. *Turbulent flows*. Cambridge University Press, Cambridge.